Karakoc, Alp; Tukiainen, Pekka; Freund, Jouni; Hughes, Mark

Experiments on the effective compliance in the radial-tangential plane of Norway spruce

Published in:
Composite Structures

DOI:
10.1016/j.compstruct.2013.03.013

Published: 01/01/2013

Document Version
Peer-reviewed accepted author manuscript, also known as Final accepted manuscript or Post-print

Please cite the original version:
Karakoc, A., Tukiainen, P., Freund, J., & Hughes, M. (2013). Experiments on the effective compliance in the radial-tangential plane of Norway spruce. *Composite Structures*, *102*, 287-293.
https://doi.org/10.1016/j.compstruct.2013.03.013

EXPERIMENTS ON THE EFFECTIVE COMPLIANCE IN THE RADIAL-TANGENTIAL PLANE OF NORWAY SPRUCE

Alp Karakoç [1,*], Pekka Tukiainen[2], Jouni Freund[1], Mark Hughes[2]

[1]*Aalto University, School of Engineering, Department of Applied Mechanics, P.O.BOX 14300, FI-00076 AALTO, FINLAND*

[2]*Aalto University, School of Chemical Technology, Department of Forest Products Technology, P.O.BOX 16400, FI-00076 AALTO, FINLAND*

ABSTRACT

Analysis and design of wood based composites and structures need reliable experimental compliance of their constituting materials. Therefore, an experimental method is presented to determine all of the effective in-plane elastic parameters and applied to Norway spruce specimens in the radial tangential *RT* plane due to the use of this species in wide variety of engineering applications. For the purpose, uni-axial compression experiments are conducted on the specimens for different material orientations under the assumptions of small strains and small rotations. Boundary extremes of the specimens are allowed to rotate for minimizing the boundary artifacts and providing near-ideal specimen deformation. During these experiments, digital image correlation is used to obtain the displacement and strain fields whilst the stress is computed through the applied load and specimen geometry. In addition to the common practice of tabulated parameters for each nominal material orientation, the experiment results are further processed through the transformation rule and least squares function. Consequently, the effective elastic parameters in the *RT* plane are obtained by taking general anisotropic linear elasticity into account and the material classification is performed. By means of the current method, it is expected to advance the effective in-plane compliance measurements of natural cellular materials.

Keywords: Compliance, Norway spruce, radial tangential plane, digital image correlation, natural cellular material.

*Corresponding author. Tel: +358 470 23442.

Email address: alp.karakoc@aalto.fi (Alp Karakoç).

1. INTRODUCTION

Due to its abundance and high stiffness-to-weight ratio, Norway spruce (*Picea abies*) is one of the most commonly used softwood species in the pulping and paper industries as well as in structural applications such as glulam beams, plywood and particle boards [1,2]. In these applications, the effective compliance in the radial tangential *RT* plane of Fig. 1 is matter of special interest due to the significance of the transverse loads [3]. Considering this issue, various numerical studies have been conducted in which the main strategy is based on the continuum models or the micromechanical models. In the continuum models, the heterogeneous medium, e.g. the cellular structure of wood, is expressed as an equivalent homogeneous medium where the geometrical and mechanical characteristics of the microscopic heterogeneities are averaged over the representative volume elements [4]. In the micromechanical models, the material is represented as a heterogeneous medium by using a discrete-beam network where direct calculations can be performed to obtain the microscopic mechanical quantities [5]. In contrast to the abundance of numerical studies that have been undertaken, there have been few experimental studies that report the deformation and measuring the effective elastic parameters in the plane of interest because the experimental calculations, especially for shear modulus, require either complicated setup than uni-axial test setup or sophisticated analysis of the raw experiment data. Therefore, in most of the experimental investigations related to the wood, the computations are performed under *a priori* assumption of orthotropy and the effective in-plane elastic parameters are determined by using just one specific material orientation, e.g. uni-axial tension/compression experiments along only radial *R* or tangential *T* directions, etc. [6, 7]. In fact, theoretically, these parameters can be obtained with the material experiments of at least three different material orientations, i.e. linearly independent homogeneous stress states [8].

In order to advance the theoretical basis of the natural cellular material testing, an experimental method, which is based on the earlier study on the cellular structures [8], is presented to obtain all of the effective in-plane elastic parameters and applied to the Norway spruce specimens in the radial tangential *RT* plane. For the purpose, uni-axial compression experiments are carried out on the specimens for different material orientations under the assumptions of small strains and small rotations. In contrast to the conventional studies, boundary extremes of the specimens are allowed to rotate, which minimizes the boundary artifacts and provides near-ideal specimen deformation. Digital

image correlation is used to obtain the displacement and strain fields whilst the stress is computed through the applied load and the specimen geometry. The analysis is confined to a measurement domain under near-homogeneous stress and strain fields. After tabulating the elastic parameters for the chosen nominal material orientations, the experiment results are further processed through the transformation rule and least squares function to determine the effective compliance of Norway spruce for the tested material size and plane. It is noteworthy that these calculations are performed under the assumption of general anisotropic linear elasticity and the material classification is done following the effective compliance analysis, which are the novelties compared to the conventional experimental studies. By means of the presented experimental method, it is expected to advance the current state of art through the measurement and generic analysis techniques.

---Preferred position for Fig. 1---

2. MATERIALS AND METHODS

2.1. Material

In the present study, experiments are carried out on the miniature Norway spruce specimens, the stem of which was obtained from Mikkeli, Finland and stored in a freezer. Two discs containing 26 growth rings is cut from the stem for the specimen preparation and dried in a climatic chamber at 20 °C and 65 % relative humidity. All the specimens are taken from the outer region of the disc (growth ring numbers 18-25, i.e. radial distance of approximately 50-80 mm from the pith). Density of the specimens is measured based on mass-to-volume ratio at approximately 13 % moisture content. These measurements indicate that the density varies between 0.39 g/cm^3 and 0.44 g/cm^3 under the controlled environment.

2.2. Theoretical background for the effective compliance analysis in the *RT* plane

Norway spruce is a softwood species which have cellular structure and anisotropic material behaviour. Its anisotropic nature is attributed to the arrangement of the wood

cells, helical structure of the cell wall layers and lay-up of cellulose fibers in the cell wall layers [9, 10]. The mechanical behaviour has been examined theoretically in various publications [11]. For the simplicity, the common analysis approach in these investigations is based on the material classification *a priori* to the experiments, thus the outcome is limited to the assumption of orthotropy. However, in the authors' opinion, the analysis should include the possibility of general anisotropic linear elastic behaviour. In this case, the effective in-plane compliance matrix is given as

$$[\underline{\mathbf{C}}] = \begin{bmatrix} 1/E_R & -\nu_{TR}/E_T & \eta_{RT,R}/E_R \\ -\nu_{RT}/E_R & 1/E_T & \eta_{RT,T}/E_T \\ \eta_{RT,R}/E_R & \eta_{RT,T}/E_T & 1/G_{RT} \end{bmatrix} \tag{1}$$

in which E_R, E_T, G_{RT}, ν_{RT}, ν_{TR} are the effective elastic moduli, shear modulus, and Poisson's ratios in the *RT* plane, respectively. Here, the coefficients of mutual influence $\eta_{RT,R}$, $\eta_{RT,T}$ characterize the coupling between shearing and normal stresses [12]. After obtaining the parameters of Eq. (1), one can clearly classify the material [13].

2.3. Theoretical background for the experiments

In these experiments, the laboratory *XY*-coordinate system and the material *RT*-coordinate system (hereafter, abbreviated as cs) are used as seen in Fig. 2. The *XY*-cs is used to describe the experiment plane in the laboratory environment, while the *RT*-cs is used to describe the radial tangential *RT* plane of the Norway spruce.

---Preferred position for Fig. 2---

In the *XY*-cs, the generic linear stress-strain relationship is constructed using the Voigt notation as

$$\{\mathbf{e}\} = [\mathbf{C}]\{\mathbf{s}\} \tag{2}$$

due to practical difficulties in using high-order tensors [12]. Curly {} and square brackets [] are the component representations of the tensors in the basis of a fixed coordinate system. In Eq. (2), {**e**} and {**s**} are the column vector representations for the strain and stress tensors with the assumption of symmetry ($e_{mn}=e_{nm}$ and $s_{mn}=s_{nm}$ for $m, n \in \{X, Y\}$)

while $[\mathbf{C}]$ is the square matrix representation for the fourth-order compliance tensor **C**. Here, it should be noted that $[\mathbf{C}]$ and $[\underline{\mathbf{C}}]$ denote the compliance in the basis of the *XY*-cs and the *RT*-cs, respectively. Then, Eq. (2) can be expanded to the component form as

$$\begin{Bmatrix} e_{XX} \\ e_{YY} \\ 2e_{XY} \end{Bmatrix} = \begin{bmatrix} C_{11} & C_{12} & C_{16} \\ C_{12} & C_{22} & C_{26} \\ C_{16} & C_{26} & C_{66} \end{bmatrix} \begin{Bmatrix} s_{XX} \\ s_{YY} \\ s_{XY} \end{Bmatrix} = [\mathbf{T}]^{\mathrm{T}} \begin{bmatrix} \underline{C}_{11} & \underline{C}_{12} & \underline{C}_{16} \\ \underline{C}_{12} & \underline{C}_{22} & \underline{C}_{26} \\ \underline{C}_{16} & \underline{C}_{26} & \underline{C}_{66} \end{bmatrix} [\mathbf{T}] \begin{Bmatrix} s_{XX} \\ s_{YY} \\ s_{XY} \end{Bmatrix} \tag{3}$$

in which the compliance symmetry is taken into account. Hence, the number of independent parameters reduces to 6 [14]. In Eq. (3), superscript T denotes the matrix transpose and $[\mathbf{T}]$ is the orthogonal transformation matrix. According to [12],

$$[\mathbf{T}] = \begin{bmatrix} \cos^2\varphi & \sin^2\varphi & 2\sin\varphi\cos\varphi \\ \sin^2\varphi & \cos^2\varphi & -2\sin\varphi\cos\varphi \\ -\sin\varphi\cos\varphi & \sin\varphi\cos\varphi & \cos^2\varphi - \sin^2\varphi \end{bmatrix} \tag{4}$$

where φ is the counterclockwise orientation angle between the *X*- and *R*-axes as shown in Fig. 2.

By means of Eqs. (3) and (4), $[\mathbf{C}]$ of any rotated coordinate system can be expressed in terms of $[\underline{\mathbf{C}}]$ in the *RT*-cs. Hence, it is enough to measure the compliance in some convenient coordinate systems. The values of $\underline{C}_{11},..,\underline{C}_{66}$ can be measured by using at least three linearly independent homogeneous stress states $s^i_{XX}, s^i_{YY}, s^i_{XY}$ for $i \in \{1, 2, 3\}$. Assuming that the corresponding strain components $e^i_{XX}, e^i_{YY}, e^i_{XY}$ are measured in some manner,

$$[\underline{\mathbf{C}}] = \left[\begin{array}{c|c|c} e^1_{XX} & e^2_{XX} & e^3_{XX} \\ e^1_{YY} & e^2_{YY} & e^3_{YY} \\ 2e^1_{XY} & 2e^2_{XY} & 2e^3_{XY} \end{array}\right] \left[\begin{array}{c|c|c} s^1_{XX} & s^2_{XX} & s^3_{XX} \\ s^1_{YY} & s^2_{YY} & s^3_{YY} \\ s^1_{XY} & s^2_{XY} & s^3_{XY} \end{array}\right]^{-1} . \tag{5}$$

However, in order to be more precise, specimens should be tested for more than three different material orientations relative to the loading direction. In this case, the parameters can be calculated as the minimizers of the least squares function

$$\pi(\underline{C}_{11},..,\underline{C}_{66}) = \sum_{i=1}^{n} \left\| \begin{Bmatrix} e^i_{XX} \\ e^i_{YY} \\ 2e^i_{XY} \end{Bmatrix} - [\mathbf{T}]^{\mathrm{T}} \begin{bmatrix} \underline{C}_{11} & \underline{C}_{12} & \underline{C}_{16} \\ \underline{C}_{12} & \underline{C}_{22} & \underline{C}_{26} \\ \underline{C}_{16} & \underline{C}_{26} & \underline{C}_{66} \end{bmatrix} [\mathbf{T}] \begin{Bmatrix} s^i_{XX} \\ s^i_{YY} \\ s^i_{XY} \end{Bmatrix} \right\|^2 \tag{6}$$

in which the matrix norm $\|\ \|$ is the Euclidean. For a unique minimizer, i.e. the values of the material parameters in Eq. (1), the number of independent equations should be equal to or exceed that of the parameters, which can be achieved with the repetitive measurements on various linearly independent homogeneous stress states.

3. EXPERIMENTS

Uni-axial compression experiments are conducted on the specimens with different material orientations relative to the loading direction as illustrated in Fig. 3. For each nominal material orientation, 10 clear wood specimens are sawn from the same disc (growth ring numbers 18-25) where the cross-sectional dimensions are 15 mm × 5 mm in the *RT* plane and thickness is 5 mm in the longitudinal *L* direction. Following the sawing process, arbitrary speckle patterns are sprayed on the specimen surfaces. These patterns are necessary for the optimal use of the digital image correlation technique which is used for measuring the displacement fields of the specimens during the experiments. The measured load and displacement data are used to calculate the strains of the measurement domains as functions of stresses and, finally, the compliance matrices of Eq. (1) describing the elastic properties of Norway spruce in the *RT* plane.

--- Preferred position for Fig. 3---

3.1. Design of experiments

The experiments are designed so that the independent variables of the experiments are the orientation angle φ and the displacement of the actuator. As depicted in Fig. 3, the nominal orientation angles φ are chosen to be $\varphi \in \{0^\circ, 15^\circ, 30^\circ, 45^\circ, 60^\circ, 75^\circ, 90^\circ\}$, the measured means and standard deviations of which are listed in Table 1. The dependent variables are the load vector $\underline{\vec{F}}$ and the displacement field of the measurement domain Ω_{m}, which are used in the stress and strain calculations and hence the effective compliance matrix in the *RT* plane.

--- Preferred position for Table 1---

3.2. Experiment setup

The experiments are conducted in a loading stage designed for the use with a light microscope (Leica Wild MZ 8 with 0.5× magnification adapter) and CCD camera (JVC KY-F55B). The loading stage shown in Fig. 4 consists of a screw-driven mechanism actuated by a small stepper motor, force transducer (HMB U9B) with the upper limit of 500 N and a displacement transducer (Solartron AX/2.5/SH) measuring the cross-head displacements. In order to provide proper condition for the uni-axial loading, the upper and lower cross-heads are constrained to move along the *Y*-axis while the rotational degree of freedom is given with additional steel cylinders between the cross-heads and gripper plates. Under this gripping condition, the likely effect of shear at the boundary extremes are minimized [15].

During the experiments, the mechanism is driven with a constant speed of 0.4 mm/min in order to avoid the activation of visco-elastic mechanisms of wood. The specimens are tested till the failure; however, the data which is obtained till the compressive load of $15\,\mathrm{N}$ is used in the analysis. In every $1\,\mathrm{N}$ load interval, the micrographs are captured with the resolution of 768 pixel × 574 pixel, where the distance between the microscope lens and the target area is adjusted to be approximately 190 mm in order to track the full-field deformation. Thereafter, these micrographs are analyzed with the digital image correlation to obtain the displacement fields in a measurement domain Ω_{m} which is smaller than the specimen. The computations for the effective in-plane compliances are performed solely inside this domain.

---Preferred position for Fig. 4---

4. ANALYSIS

4.1. Digital image correlation

Digital image correlation is an optical-numerical displacement measurement technique, which is based on the comparison between the captured micrographs during the material testing. The technique is widely used in the field of experimental mechanics and has also been used for measuring the displacement and strain fields of different wood

species [16-19]. For the optimal use of the correlation technique, the tested specimen has to be covered with the painted arbitrary speckles. Although the transversal section of spruce at certain scale has a texture that acts as random speckle, sprayed speckle pattern enhances the contrast and improve the accuracy of digital image correlation results.

The displacement and strain fields are computed by means of MatPIV v.1.6.1-computer code, which was written for particle image analysis and is run in Matlab environment [20]. In the analysis, subset size is decided to be 40 pix × 40 pix, which corresponds to the spatial resolution of 0.9 mm × 0.9 mm. In Fig. 5, subset centers are indicated with the markers forming the predefined measurement domains Ω_{m}.

---Preferred position for Fig. 5---

4.2. Strain and stress measures

The center coordinates of subset i (X_i^f, Y_i^f) associated to frame f in situ are directly obtained through the digital image correlation measurements for Ω_{m} of Fig. 5. By using the data, average displacements of the subsets for frame f are obtained as

$$\begin{Bmatrix} u_{Xi}^f \\ u_{Yi}^f \end{Bmatrix} = \begin{Bmatrix} X_i^{f+1} - X_i^f \\ Y_i^{f+1} - Y_i^f \end{Bmatrix} \tag{7}$$

in which u_X, u_Y are the displacement components in the directions of the X- and Y-axes, respectively. The displacements in Eq. (7) are used to calculate the continuous linear displacement field $\vec{u}^f$. In component form,

$$\begin{Bmatrix} u_X^f \\ u_Y^f \end{Bmatrix} = \begin{bmatrix} p_1^f & p_2^f & p_3^f \\ p_4^f & p_5^f & p_6^f \end{bmatrix} \begin{Bmatrix} 1 \\ X \\ Y \end{Bmatrix} \tag{8}$$

where p_j^f for $j \in \{1, 2, .., 6\}$ are the polynomial coefficients. Since the homogeneous strain field is considered in the measurement domain of each frame, only first order polynomials are used. Here, p_j^f for $j \in \{1, 2, .., 6\}$ are the minimizers of least squares function

$$\pi(p_1^f,\, p_2^f, \ldots) = \sum_{i=1}^{n} \left\| \begin{Bmatrix} u_{Xi}^f \\ u_{Yi}^f \end{Bmatrix} - \begin{bmatrix} p_1^f & p_2^f & p_3^f \\ p_4^f & p_5^f & p_6^f \end{bmatrix} \begin{Bmatrix} 1 \\ X_i^f \\ Y_i^f \end{Bmatrix} \right\|^2 \tag{9}$$

in which the sum is over *n* markers. These coefficients are separately calculated for each frame. Hereafter, superscript f is excluded for the simplicity in the notation.

Once $\vec{u}$ of Eq. (8) is calculated, the components of the small strain tensor $\boldsymbol{\varepsilon}$ are given as

$$\begin{Bmatrix} \varepsilon_{XX} \\ \varepsilon_{YY} \\ 2\varepsilon_{XY} \end{Bmatrix} = \begin{Bmatrix} \partial u_X / \partial X \\ \partial u_Y / \partial Y \\ \partial u_X / \partial Y + \partial u_Y / \partial X \end{Bmatrix}. \tag{10}$$

The stress tensor $\boldsymbol{\sigma}$ is calculated in terms of the surface traction (force/area) and normal vectors under the assumptions of small strains and small rotations. Eventually, the components of $\boldsymbol{\varepsilon}$ and $\boldsymbol{\sigma}$ are replaced with **e** and **s** of Eq. (2) for calculating the effective in-plane compliance.

5. RESULTS AND DISCUSSIONS

5.1. Compression experiments

Uni-axial compression experiments are carried out to analyze the elastic material behavior of the Norway spruce specimens in the *RT* plane. During these experiments, the load and cross-head displacement data are obtained with the aforementioned measurement system, and the typical load-displacement curve for a specimen with the nominal material orientation $\varphi = 45^\circ$ is shown in Fig. 6.

Based on the procedure proposed for the off-axis material experiments in [15], the experiment setup is designed to allow the rotation of the boundary extremes and provide near-ideal specimen deformation. In order to examine the constraints, the micrographs of the abovementioned specimen are captured under two different load levels within and beyond the load range used in the analysis, which are (I): 10 N and (II): 25 N. As depicted in Fig. 6, the comparison of the angles between the boundary extremes and the *Y*-axis indicates the existence of rotations provided by the gripper plates. According to

this investigation, both the assumption of small rotations and the gripping condition are valid within the focused load range.

---Preferred position for Fig. 6---

5.2. Effects of the measurement domains

The first notable outcome of this experimental study is the stress-strain relationship which is computed for several measurement domains in each material orientation. By means of the investigation on different domains, it is aimed to understand the possible effects of boundary artifacts and determine the convenient measurement domain under near-homogeneous stress and strain fields. For this purpose, stress-strain curves for some of the selected nominal material orientations $\varphi \in \{0^\circ, 45^\circ, 90^\circ\}$ are shown in Fig. 7. In these analyses, two different measurement domains which are approximately 280 pix × 200 pix (Domain 1) and 600 pix × 200 pix (Domain 2) are taken into consideration. The stress-strain curves in Fig. 7 indicate that there are slight differences between the strain measurements for the domains regardless of φ, which means that the boundary artifacts can be successfully minimized in each material orientation by allowing the rotations of the gripper plates of Fig. 4 at the boundary extremes and near-ideal specimen deformation is achieved. However, to ensure a safe procedure, it is proposed to confine the measurements to the smaller domain, i.e. Domain 1, and perform the effective in-plane compliance analysis.

---Preferred position for Fig. 7---

5.3. Dependency of the elastic parameters on the material orientation

As seen in Fig. 7, all three effective in-plane strain components are measured for each tested specimen. By means of these data, it is possible to determine the elastic modulus in the direction of the uni-axial load $E_Y = s_{YY}/e_{YY}$ and the Poisson's ratio $\nu_{YX} = -e_{XX}/e_{YY}$. Thereafter, it is possible to analyze the effect of material orientation φ on the mean values of these measurable material parameters. As listed in Table 2, there is a relationship between the values of φ and E_Y, which can be explained with the

deformation mechanisms on the cellular level, i.e. cell wall bending and stretching. Analogous to the other softwood species, Norway spruce also behaves as a bending-dominated cellular material at $\varphi = 0^\circ$, i.e. deformation along tangential *T* direction (see Fig. 3), and a stretch-dominated cellular material at $\varphi = 90^\circ$, i.e. deformation along radial *R* direction (see Fig. 3), because of its cell tessellation in the form of over-expanded honeycomb material [21, 22]. In addition to this, radial alignment of the ray cells, which is originated from the natural pattern of the tree growth, acts as a barrier against the radial deformation and contributes to the stiffness along the *R* direction [23]. Similar trend is observed for ν_{YX} because of higher material rigidity along the *R* direction compared to the *T* direction.

---Preferred position for Table 2---

In addition to the analysis on the mean values of the elastic parameters in Table 2, the investigations of the standard deviations point out the possible issues related to the loading conditions and the specimens. Principally, eccentric loads not acting through the centerline of the specimens, dimensional variations in specimen cutting, misarranged material orientations and growth ring curvature due to the natural tree pattern are some of the possible reasons for the measured deviations [15].

5.4. Effective elastic parameters of Norway spruce in the *RT* plane

Although the experiments are carried out till the specimen failure, the region of interest is the linear elastic part of the stress-strain curves, some of which are provided in Fig. 7. Within this range, the measured $\boldsymbol{\varepsilon}$ and $\boldsymbol{\sigma}$ for different nominal material orientations $\varphi \in \{0^\circ, 15^\circ, 30^\circ, 45^\circ, 60^\circ, 75^\circ, 90^\circ\}$ are processed with the transformation rule and the least squares function of Eq. (6) to determine the effective compliance in the plane of interest. It is noteworthy that the measurement errors are minimized with the digital image correlation in replacement of the conventional displacement measuring equipments such as the strain gauges and linear variable differential transformer LVDT, whereas the analysis errors are minimized with the repetitive experiments. As a result of these measurements and analysis, the effective elastic parameters of Norway spruce in the *RT* plane are calculated as the minimizers of Eq. (6) and listed in Table 3. For the

evaluation purpose, the measured values are compared with the ones obtained for the same material and similar densities in the literature.

---Preferred position for Table 3---

The first notable outcome of Table 3 is the measured density of the present study, which varies between 0.39 g/cm^3 and 0.44 g/cm^3 for the selected position of the specimens, i.e. radial distance of 50-80 mm from the pith. The relationship between the radial position and density has consistency with the radial density profile for spruce provided in the literature [26]. Other notable outcomes of these measurements are the coefficients of mutual influence $\eta_{RT,R}$, $\eta_{RT,T}$ which are used to classify the material. If these are equal to zero, the material is considered as orthotropic, which represents a particular type of anisotropy. As seen in Table 3, $\eta_{RT,R}$ and $\eta_{RT,T}$ are close to zero, which means that the material used in this study can be classified as orthotropic and the selected *RT*-cs serves as the principal material coordinate system.

The comparison of the present and previous measurements in Table 3 shows that the parameters of the present study lie in the range determined by the previous studies. However, there is a wide range of the parameter values in the literature. In authors' opinion, this is related to the intrinsic properties of the investigated tree stem, selection of the specimens from different radial positions in the growth ring and the specimen dimensions. In addition to the structural variations, the measurement and analysis techniques of the conventional experiments including the strain gauges and LVDT are the other factors affecting the results [8].

Despite the differences in the measured data of Table 3, the relationship between the elastic moduli E_R, E_T in radial *R* and tangential *T* directions, i.e. $E_R > E_T$, is obvious. Hence, it can be deduced that the material has higher rigidity along the *R* direction, the reason of which has been explained in the previous section. There is a similar trend between the Poisson's ratios ν_{RT} and ν_{TR}, i.e. $\nu_{RT} > \nu_{TR}$, which indicates the anisotropic behavior of the material. The tabulated results also show that the density has directly proportional effect on the shear modulus G_{RT}, which is attributed to the increasing cell wall thicknesses.

6. CONCLUSIONS

The analysis and design of wood based composites and structures need reliable experimental compliance of their constituting materials. Therefore, an experimental analysis is presented for measuring the effective compliance matrices of Norway spruce in the radial tangential *RT* plane due to the use of this wood species in wide variety of engineering applications. In contrast to the previous studies in the literature, *a priori* assumptions regarding the geometrical and mechanical characterizations are avoided. Instead, general anisotropic linear elasticity is taken into consideration and material classification is done based on the measured elastic parameters. Hence, in addition to determination of the effective in-plane elastic moduli and the Poisson's ratios, shear modulus and mutual influence terms characterizing the coupling between shearing and normal stresses are measured.

In order to determine the effective in-plane elastic parameters, uni-axial compression experiments are performed for seven different nominal material orientations relative to the loading directions. During these experiments, boundary extremes are allowed to rotate, which minimizes the boundary artifacts and provides near-ideal specimen deformation. Still, the measurement domain for each specimen is defined far away from the boundary domains to ensure a safe procedure. The measured stress and strain data in the measurement domains are first tabulated in terms of the elastic modulus along the direction of the load and the corresponding Poisson's ratio in order to understand the dependency of these elastic parameters on the material orientation. This tabulated data show that the cell alignments and tessellation have significant effects on the deformation mechanisms and therefore the elastic material behavior.

In addition to the common practice of listing the elastic parameters of the tested material orientations, the strain and stress data are further processed with the transformation rule and least squares function. It is noteworthy that the measurement errors are minimized with the digital image correlation in replacement of the conventional displacement measuring equipments such as linear variable differential transformer LVDT, whereas the analysis errors are minimized with the repetitive experiments. As a result, the effective in-plane compliance is calculated with the minimum practical error. Analysis of the compliance shows that the tested material can be classified as orthotropic material and the selected material coordinate system serves

as the principal material coordinate system.

For the comparison purpose, the measured parameters are listed with the ones obtained in the literature. This comparative study reveals that the material has higher rigidity along the radial *R* direction compared to the tangential *T* direction resulting in the relationships $E_R > E_T$ and $\nu_{RT} > \nu_{TR}$. The comparison between the present and previous measurements also shows that the density has directly proportional effect on the shear modulus G_{RT}, which is attributed to the increasing cell wall thicknesses.

ACKNOWLEDGEMENTS

In preparation of the present article, AK has been in charge of the analysis and constructing the paper, and PT has been in charge of the experiments as well as writing the corresponding sections. The invaluable comments of D.Sc. Kari Santaoja are deeply appreciated. The authors gratefully acknowledge the financial support of Multidisciplinary Institute of Digitalisation and Energy (MIDE) through Energy Efficient Wood Processing and Machining Project (E-wood) at Aalto University and the Ministry of Education of Finland through the National Graduate School in Engineering Mechanics.

REFERENCES

[1] Hassel BI, Berard P, Modén CS, Berglund LA. The single cube apparatus for shear testing – Full-field strain data and finite element analysis of wood in transverse shear. Composites Sci Technol 2009; 69: 877-82.

[2] Dahl KB. Mechanical properties of clear wood from Norway spruce. Doctoral dissertation, Trondheim, Norwegian University of Science and Technology; 2009.

[3] Garab J, Keunecke D, Hering S, Szalai J, Niemz P. Measurement of standard and off-axis elastic moduli and Poisson's ratios of spruce and yew wood in the transverse plane. Wood Science and Technology 2010; 44: 451-64.

[4] Nemat-Nasser S, Hori M. Micromechanics: Overall Properties of Heterogeneous Materials, 2nd Ed.: North Holland; 1999.

[5] Landis E, Vasic S, Davids W, Parrod P. Coupled experiments and simulations of microstructural damage in wood. Experimental Mechanics 2002; 42: 389-94.

[6] Jernkvist L, Thuvander F. Experimental determination of stiffness variation across growth rings in Picea abies. Holzforschuing 2001; 55: 309-17.

[7] Farruggia F, Perré P. Microscopic tensile tests in the transverse plane of earlywood and latewood parts of spruce. Wood Science and Technology 2000; 34: 65-82.

[8] Karakoç A, Freund J. Experimental studies on mechanical properties of cellular structures using Nomex® honeycomb cores. Composite Structures 2012; 94: 2017-24.

[9] Gibson L, Ashby M. Cellular solids: structure and properties. Cambridge: Cambridge University Press; 1999.

[10] Holmberg S, Persson K, Petersson H. Nonlinear mechanical behaviour and analysis of wood and fibre materials. Comput Struct 1999; 72: 459-80.

[11] Yang G, Kabel J, van Rietbergen B, Odgaard A, Huiskes R, Cowin SC. The anisotropic Hooke's law for cancellous bone and wood. J Elast 1998; 53: 125-46.

[12] Jones R. Mechanics of Composite Materials. Washington, D.C.: McGraw-Hill Book Company; 1975.

[13] Felippa CA, Oñate E. Stress, strain and energy splittings for anisotropic elastic solids under volumetric constraints. Comput Struct 2003; 81: 1343-57.

[14] Kaw A. Mechanics of Composite Materials, 2nd Ed. Boca Raton: Taylor-Francis Group; 2006.

[15] Marin JC, Canas J, Parıis F, Morton J. Determination of G12 by means of the off-axis tension test.: Part I: review of gripping systems and correction factors. Composites Part A: Applied Science and Manufacturing 2002; 33: 87-100.

[16] Samarasinghe S, Kulasiri D. Displacement fields of wood in tension based on image processing: Part 1. Silva Fenn 2000; 34: 251-9.

[17] Samarasinghe S, Kulasiri D. Displacement fields of wood in tension based on image processing: Part 2. Crack-tip displacements in mode-I and mixed-mode fracture. Silva Fenn 2000; 34: 261-74.

[18] Samarasinghe S, Kulasiri D, - Nicolle K. Study of Mode-I and Mixed-mode Fracture in Wood Using Digital Image Correlation Method. Engineering 4 1996: 144-51.

[19] Samarasinghe S, Kulasiri D. Stress intensity factor of wood from crack-tip displacement fields obtained from digital image processing. Silva Fenn 2004; 38: 267-78.

[20] Sveen J. An introduction to MatPIV 1.6.1. Eprint no. 2. Department of Mathematics, University of Oslo; 2004.

[21] Deshpande VS, Ashby MF, Fleck NA, Foam topology: bending versus stretching dominated architectures, Acta Materialia 2001; 49: 1035-40.

[22] Vural M, Alkhader M. Mechanical response of cellular solids: Role of cellular topology and microstructural irregularity. International Journal of Engineering Science 2008; 46: 1035–51.

[23] Kahle E, Woodhouse J. The influence of cell geometry on elasticity of softwood. Journal of Materials Science 1994; 29: 1250-9.

[24] Carrington H. The elastic constants of spruce. Phil. Mag. 1923; 45: 1055-7.

[25] Kollmann F, Côté W. Principles of Wood Science and Technology - Solid Wood, 1st Ed. Berlin: Springer Verlag; 1968.

[26] Moden CS, Berglund LA, "Elastic deformation mechanisms of softwoods in radial tension - Cell wall bending or stretching?". Holzforschung 2008; 62: 562-8.

Table 1: Measured means and standard deviations of the nominal orientation angles φ.

	Nominal orientation angle φ (º)						
Sample	0	15	30	45	60	75	90
Mean	5.1	15.7	29.6	47.4	58.3	74.2	90.9
St.Dev.	0.9	2.9	3.1	0.9	3.0	2.1	1.9

Table 2: Angular dependency of the measured effective elastic parameters in the *XY*-cs.

		Nominal orientation angle φ (°)						
	Sample	0	15	30	45	60	75	90
E_Y (MPa)	Mean	437.5	362.5	140.1	148.1	172.7	472.5	933.4
	St.Dev.	33.6	16.7	2.9	6.8	12.5	28.8	80.2
ν_{YX}	Mean	0.34	0.64	0.83	0.90	0.91	0.86	0.64
	St.Dev.	0.02	0.07	0.02	0.01	0.01	0.02	0.01

Table 3: Effective elastic parameters of Norway spruce in the *RT* plane.

	Density (g/cm^3)	E_R (MPa)	E_T (MPa)	G_{RT} (MPa)	ν_{RT}	ν_{TR}	$-\eta_{RT,R}$	$-\eta_{RT,T}$
Present study	0.39-0.44	955	411	25	0.62	0.27	0.094	0.061
Survey-I [23]	0.37-0.55	640-890	360-630	22-37	0.43-0.64	0.25-0.33	---	---
Survey-II [24]	0.39	640	420	26	0.64	0.32	---	---
Survey-III [25]	0.44-0.50	690-810	390-630	35-36	0.42-0.43	0.24-0.33	---	---

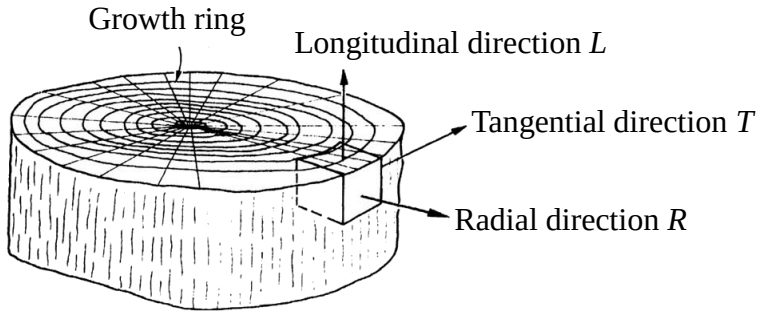

Figure 1: Material coordinate system attributed to the structural features in a tree stem. The radial tangential *RT* plane, which is also termed as transverse plane after Gibson and Ashby [9], is matter of interest.

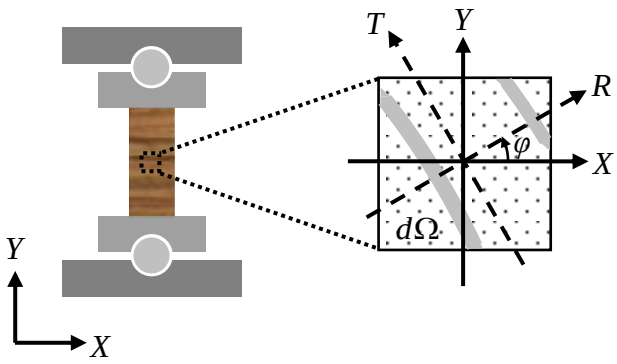

Figure 2: Specimen and the coordinate systems. Here, φ is the counterclockwise orientation angle between X- and R-axes and $d\Omega$ is the infinitesimal domain.

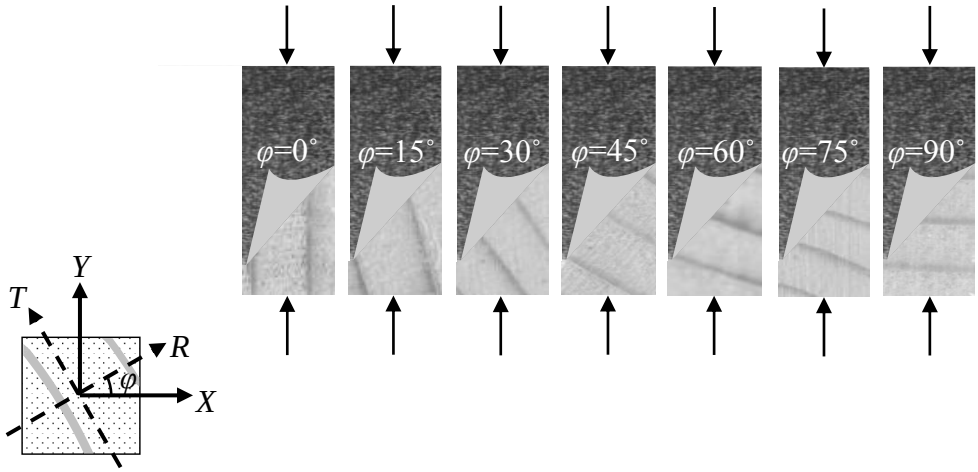

Figure 3: Specimens of different nominal material orientations relative to the uni-axial compressive loading.

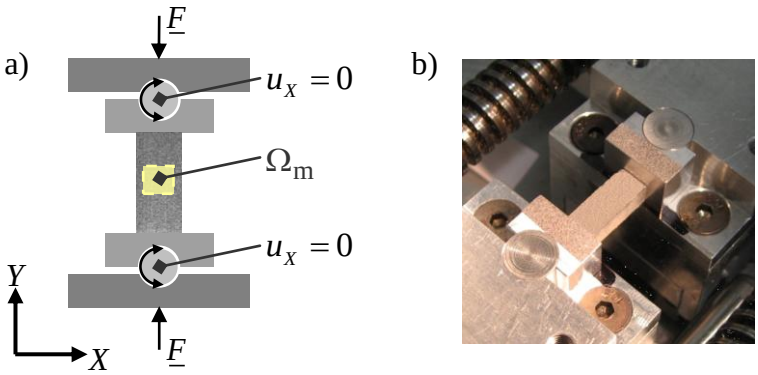

Figure 4: Experiment setup: a) schematic representation of the loading and boundary conditions, and the measurement domain, b) loading stage. Here, u_X is the displacement component in the direction of the *X*-axis.

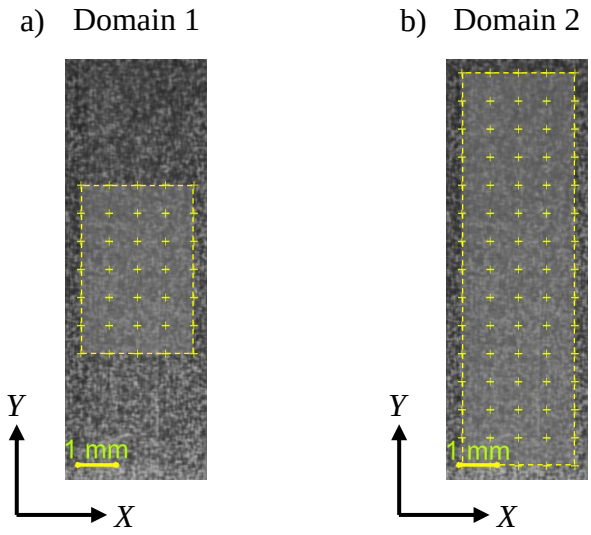

Figure 5: Specimen with speckle pattern and the markers indicating the subset centers on the predefined measurement domains: a) 280 pix × 200 pix, b) 600 pix × 200 pix.

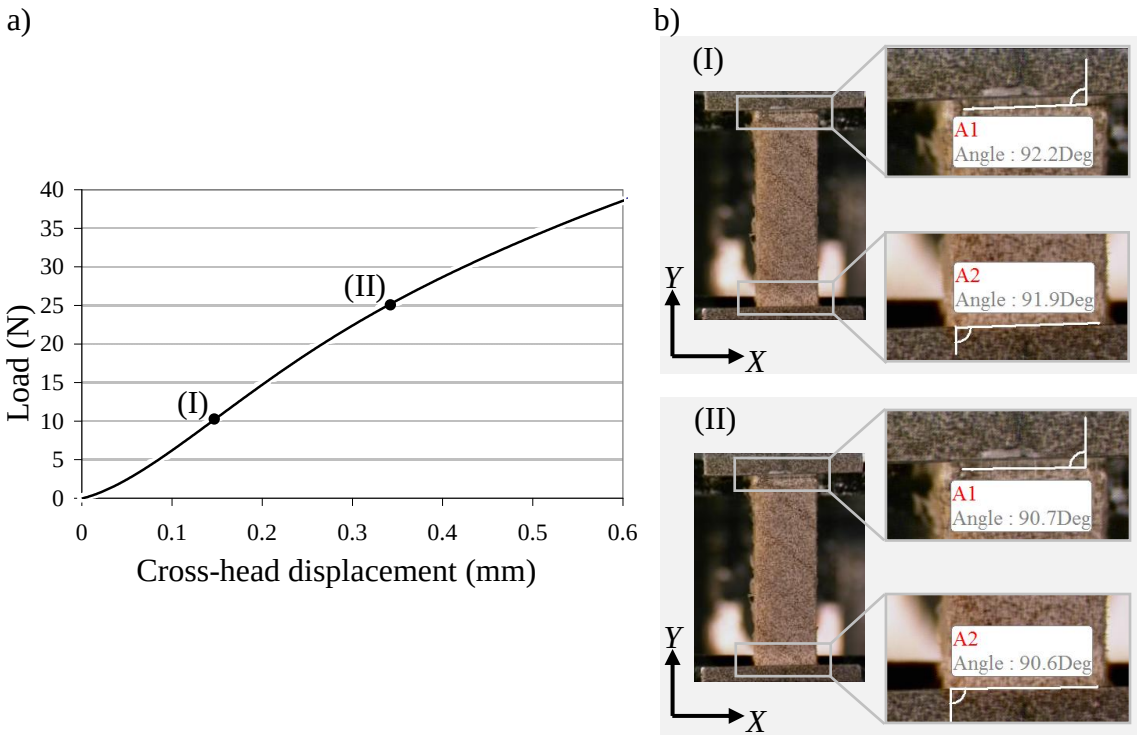

Figure 6: Specimen deformation under the uni-axial compressive load along the *Y*-axis: a) load-displacement curve for the specimen with $\varphi = 45^{\circ}$, b) rotation angles of the boundary extremes with respect to the *Y*-axis under different load levels.

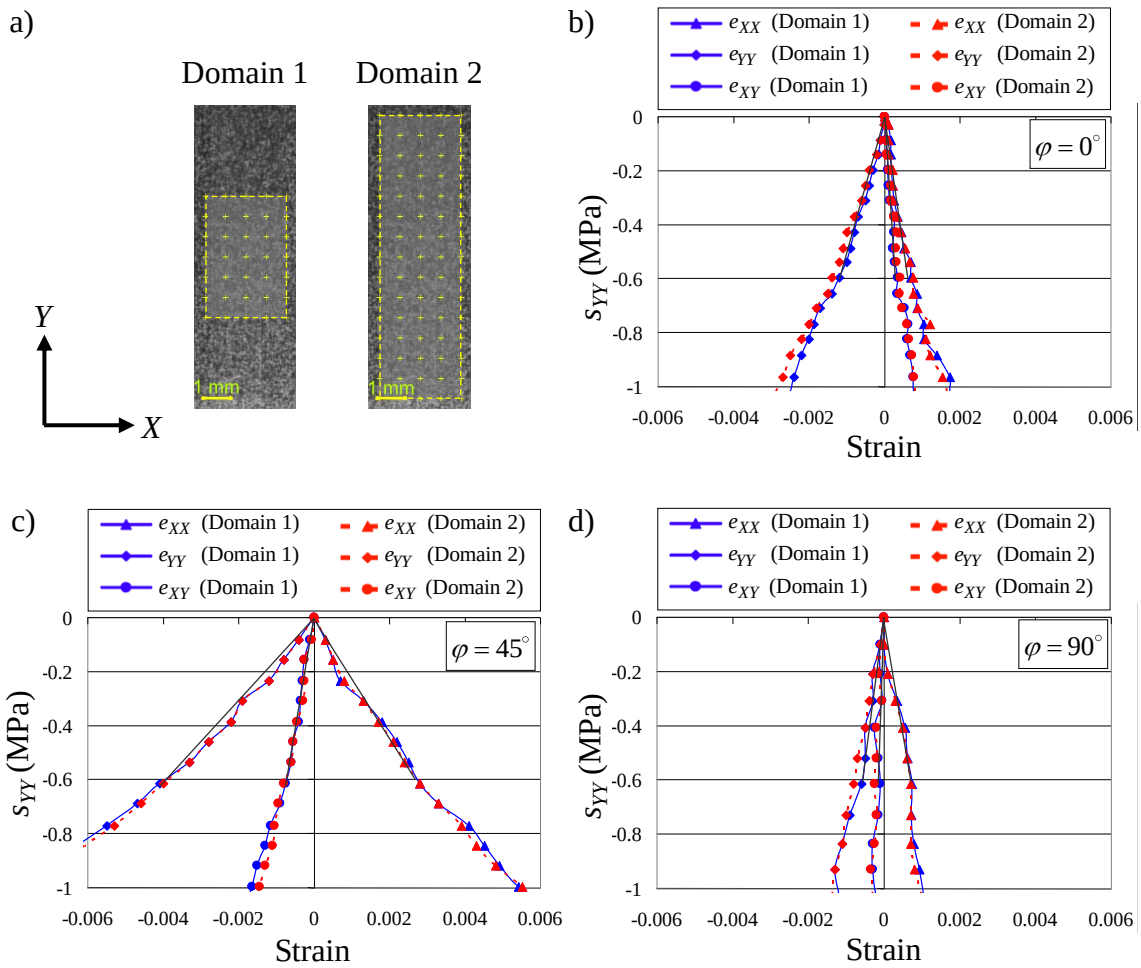

Figure 7: Specimen deformation under the uni-axial compressive load along the *Y*-axis: a) predefined measurement domains on the speckle pattern, b) stress-strain curve for the specimen with $\varphi = 0^{\circ}$, c) stress-strain curve for the specimen with $\varphi = 45^{\circ}$, and d) stress-strain curve for the specimen with $\varphi = 90^{\circ}$.